OTKA 83023 “Proteolytic destruction of the thrombus matrix: characterization of new targets and tools for thrombolysis”
FINAL REPORT

The results of the project have been published in 15 original papers with a total impact factor of 63.533 and 3 book chapters, in which the support received from the OTKA has been acknowledged. In addition, 23 abstracts were presented as talks or posters at national and international scientific congresses organised by the International Society on Thrombosis and Haemostasis, the International Society on Fibrinolysis and Proteolysis, the Hungarian Society on Thrombosis and Haemostasis, the European Society of Cardiology and there are some unpublished results that are summarized in the Appendix of this final report. The impact of the performed research is reflected in the number of independent citations (105) received for the papers published within the framework of the completed project. Three of the publications were commended in editorial comments of the respective journals. Accordingly, instead of self-evaluation the opinion of these independent experts is cited below to illustrate the major outcomes of the research. Concerning our **paper #1 John Weisel** wrote the following in ***Journal of Thrombosis and Haemostasis*** (2011;9:977-978): “Although novel but physiologically important factors that affect fibrinolysis have seldom been discovered and characterized in recent years, yet in this issue of the Journal of Thrombosis and Haemostasis there is such a report [1]. This study demonstrates that the lytic susceptibility of fibrin under mechanical stress is greatly reduced. It is also another indication of the importance of biomechanics in hemostasis and yet how little we still know of this area of research [2,3]. This paper presents a good example of how science should work: one study stimulates important new research in other, unforeseen directions. From an investigation of the origins of the mechanical properties of fibrin [4], including stretching of clots, arises the basic question: What is the effect of stretching of fibrin on fibrinolysis? The results of experiments reported here answer that question and at the same time provide a first step toward solving the long-standing mystery of the extreme resistance of some thrombi and retracted clots to lysis [5–7]. Clinically, these results also account at least in part for the fact that thrombolytic drugs are less effective at longer times after thrombi are formed, perhaps due to their mechanical deformation.” Concerning our **paper #2 Bernd Engelmann** wrote the following in ***Thrombosis and Haemostasis*** (2015; 113: 1164): “The study by Varjú et al. (4) adds a new aspect to the procoagulant role of nucleosome components and NETs. These authors show that isolated eukaryotic DNA and histone proteins such as HIIIS enhance the diameter of thrombus-forming fibrin fibers under *in vitro* conditions. Moreover, they are found to decrease the permeability of fibrin clots and to enhance the overall stability of such clots. Mechanistically, these effects are mediated by regulation of endogenous anticoagulant and fibrinolytic pathways. Indeed, histone proteins prevented the inactivation of thrombin by antithrombin and DNA reduced plasminogen activation. Furthermore, NETs released from isolated neutrophils suppressed t-PA-promoted fibrinolysis. Together with earlier work, these results further corroborate the conclusion that extracellular nucleosomes and their major components target the coagulation system at different levels and that their overall effect is to enhance fibrin formation.” Concerning our **paper #3 Helen Philippou** wrote the following in ***Thrombosis Research*** (2014; 113:1-2): “The current study by Kovacs et al in this issue, provides further evidence that TAFI function may not be as straight-forward as was originally considered for its role in the down-regulation of fibrinolysis. Hence, the contribution of carboxypeptidase to fibrin structure during ongoing clot formation and fibrinolysis provides a novel mechanism for the regulation of fibrinolysis that does not depend directly on C-terminal lysine cleavage and reduction in binding sites for plasminogen and tPA. Intriguingly, arginine present during fibrin formation was also found to replicate some of these effects. This study is therefore the first to suggest that TAFI is capable of enhancing fibrinolysis; changing our current understanding of the role of TAFI in fibrinolysis, dependent upon the circumstances of fibrinolysis/fibrin formation.” These examples clearly demonstrate the novelty and significance of three highlighted results from the research performed within the framework of the completed project.

The results published in our **paper #4** received most attention during the project (40 independent citations). In this study we evaluated how the regulation of tissue-type plasminogen activator (tPA) depends on fibrin binding and fibrin structure. tPA structure/function relationships were investigated in fibrin formed by high or low thrombin concentrations to produce a fine mesh and small pores, or thick fibres, and coarse structure, respectively. Kinetics studies were performed to investigate plasminogen activation and fibrinolysis in the 2 types of fibrin, using wild type tPA, (F-G-K1-K2-P, F and K2 binding), K1K1tPA (F-G-K1-K1-P, F binding) and delF-tPA (G-K1-K2-P, K2 binding). There was a trend of enzyme potency of tPA>K1K1tPA>delFtPA highlighting the importance of the finger domain in regulating activity, but the differences were less apparent in fine fibrin. Fine fibrin was a better surface for plasminogen activation but more resistant to lysis. Scanning electron and confocal microscopy using orange fluorescent fibrin with green fluorescent protein (GFP)-labelled tPA variants showed that tPA was strongly associated with agglomerates in coarse but not in fine fibrin. In later lytic stages delF-tPA-GFP diffused more rapidly through fibrin in contrast to full length tPA, highlighting the importance of finger domain-agglomerate interactions. Thus, the regulation of fibrinolysis depends on the starting nature of fibrin fibres and complex dynamic interaction between tPA and fibrin structures that vary over time. Furthermore, finger-dependent focalization on cross-β structures in coarse fibrin agglomerates generated primarily at the fibrin surface during fibrinolysis, may represent a previously underappreciated, distinct mechanism of tPA binding that has important implications for the regulation of fibrinolysis.

Another line of research that received significant attention was the role of cellular elements as determinants of fibrin structure and of the mechanical and lytic stability of the clots, our work with red blood cells (RBC, **paper #5**) and neutrophil extracellular traps (NETs, **paper #6**) has been cited 34 times in independent publications. In paper #5 we evaluated the modulator role of RBCs in the lytic susceptibility of fibrin. We showed that arterial thrombi contain variable amounts of RBCs, which interact with fibrinogen through an eptifibatide-sensitive receptor and modify the structure of fibrin. If fibrin is formed at increasing RBC counts, scanning electron microscopy evidenced a decrease in fiber diameter from 150 nm to 96 nm at 40 %(v/v) RBC, an effect susceptible to eptifibatide inhibition (restoring 140 nm diameter). RBC prolonged the lysis time in a homogeneous-phase fibrinolytic assay with tissue plasminogen activator (tPA) by up to 22.7±1.6 %, but not in the presence of eptifibatide. Confocal laser microscopy using green fluorescent protein (GFP)-labeled tPA and orange fluorescent fibrin showed that 20-40 %(v/v) RBC significantly slowed down the dissolution of the clots. tPA-GFP did not accumulate on the surface of fibrin containing RBC at any cell count above 10 %. The presence of RBC in the clot suppressed the tPA-induced plasminogen activation resulting in a 45 % less plasmin generated after 30 min activation at 40 %(v/v) RBC. Thus, our study was the first to describe that RBCs confer lytic resistance to fibrin resulting from modified fibrin structure and impaired plasminogen activation through a mechanism that involves eptifibatide-sensitive fibrinogen-RBC interactions. Our paper #6 was the first to report the presence of NETs in arterial thrombi as a secondary matrix complementary to the fibrin scaffold, we detected NETs in thrombi removed with surgery from patients with peripheral arterial disease. NETs are networks of DNA and associated proteins produced by nucleosome release from activated neutrophils in response to infection stimuli and have recently been identified as key mediators between innate immunity, inflammation and hemostasis. The interaction of DNA and histones with a number of hemostatic factors has been shown to promote clotting and is associated with increased venous thrombosis, but little was known about the effects of DNA and histones on the regulation of fibrin stability and fibrinolysis. Our experiments showed that the addition of histone - DNA complexes to fibrin results in thicker fibers (increase in median diameter from 84 to 123 nm according to scanning electronmicroscopic data) which is accompanied by improved stability and rigidity (the critical shear stress causing loss of fibrin viscosity increases from 150 to 376 Pa, whereas the storage modulus of the gel increases from 62 to 82 Pa according to oscillation rheometric data). Small angle X-ray scattering (SAXS) analysis indicated that DNA or heparin

disrupt the regular longitudinal alignment of the monomeric building blocks of fibrin. In contrast, the addition of histone does not interfere with the longitudinal periodicity, the related scattering peak is even more pronounced. The SAXS peak attributed to periodicity of ~12.5 to 31 nm in cluster units of the fibers and the one corresponding to periodicity of ~4 to 10 nm characteristic for the average protofibril-to-protofibril distance were most profoundly affected by the presence of histone suggesting that this additive interferes with the lateral organization of protofibrils resulting in lower protofibril density. The effects of DNA and histones alone are subtle and suggest histones affect clot structure whereas DNA changes the way clots lyse. The combination of histones + DNA significantly prolongs clot lysis. Isothermal titration and confocal microscopy studies suggest histones and DNA bind large fibrin degradation products with 191 and 136 nM dissociation constants, respectively, interactions which stabilise lysing clots. Heparin, which is known to interfere with the formation of NETs, appears to prolong lysis time at concentration favouring ternary histone-DNA-heparin complex formation and DNase effectively promotes clot lysis in combination with tissue plasminogen activator. This work was expanded later to a more complex system in plasma environment as discussed above in relation to paper #2.

In addition to the fibrin and NET matrix, von Willebrand factor (VWF) multimers, bridging platelet membranes also stabilize the structure of thrombi. Our **paper #7** addressed the role of hemostatic-fibrinolytic enzymes (thrombin, plasmin) and leukocyte-derived proteases (matrix metalloproteinase (MMP)-8, MMP-9, neutrophil elastase) in the cleavage of VWF and the effect of flow and platelets on this proteolysis and its functional consequences on platelet adhesion. According to VWF immunoblots, plasmin, neutrophil elastase and thrombin at concentrations of *in vivo* relevance resulted in extensive degradation of VWF within several minutes. Platelets protected VWF against this proteolysis under static conditions, whereas perfusion of the proteases at 3350 s^{-1} shear rate over VWF immobilized on artery cross sections enhanced its degradation and blocked the protective effect of platelets. In parallel with VWF digestion, the examined proteases impaired the VWF-dependent platelet adhesion as reflected in the decreased surface-bound GpIIb/IIIa immunoreactivity following perfusion of collagen-coated surfaces or artery sections with blood and plasmin, neutrophil elastase or thrombin. Within the time frame of minutes no VWF cleavage could be detected under static or flow conditions after exposure to MMP-8 and MMP-9 at concentrations relevant to physiological neutrophil counts. Our results indicated a shear- and platelet-dependent role for several proteases in the local modulation of the VWF function.

In addition to the release of NETs, leukocytes are a source of proteases expressed in atherosclerotic plaque lesions and these generate collagen fragments, release glycosaminoglycans (chondroitin sulfate CS, dermatan sulfate DS) and expose extracellular matrix (ECM) proteins (e.g. decorin) at sites of fibrin formation as summarized in our review **paper #8**. Based on these facts in our **paper #9** we addressed the effect of vessel wall components on the lysis of fibrin by the tPA/plasminogen system and on the mechanical stability of clots. MMP-8-digested collagen fragments, isolated CS, DS, glycosylated decorin and its core protein were used to prepare mixed matrices with fibrin (additives present at a 50-fold lower mass concentration than fibrinogen). Scanning electron microscopy showed that the presence of ECM components resulted in coarse fibrin structure, most pronounced for glycosylated decorin causing increase in the median fiber diameter from 85 to 187 nm. Rheological measurements indicated that these structural alterations were coupled to decreased shear resistance (1.8-fold lower shear stress needed for gel/fluid transition of the clots containing glycosylated decorin) and rigidity (reduction of the storage modulus from 54.3 to 33.2 Pa). The lytic susceptibility of the modified fibrin structures was increased. The time to 50 % lysis by plasmin was reduced approximately 2-fold for all investigated ECM components (apart from the core protein of decorin which produced a moderate reduction of the lysis time by 25 %), whereas fibrin-dependent plasminogen activation by tPA was inhibited by up to 30 %. Our work indicated that

ECM components compromise the chemical and mechanical stability of fibrin as a result of changes in its ultrastructure, thus opposing the stabilizing effects of NETs.

In our **paper #10** a new theoretical model to evaluate fibrinolysis in quantitative enzymological terms was developed. Intravascular fibrin clots are resolved by plasmin acting at the interface of gel-phase substrate and fluid-borne enzyme. The classic Michaelis-Menten kinetic scheme cannot describe satisfactorily this heterogeneous-phase proteolysis, because it assumes homogeneous well-mixed conditions. A more suitable model for these spatial constraints, known as fractal kinetics, includes a time-dependence of the Michaelis coefficient $K_m^F=K_{m0}^F.(1+t)^h$, where h is a fractal exponent of time, t. Our aim was to build up and experimentally validate a mathematical model for surface-acting plasmin that can contribute to a better understanding of the factors that influence fibrinolytic rates. The kinetic model was fitted to turbidimetric data for fibrinolysis under various conditions. The model predicted K_{m0}^F=1.98 μM and h=0.25 for fibrin composed of thin fibers and K_{m0}^F=5.01 μM and h=0.16 for thick fibers in line with a slower macroscale lytic rate (due to stronger clustering trend reflected in the h value) despite faster cleavage of individual thin fibers (seen as lower K_{m0}^F). ε-Aminocaproic acid at 1 mM or 8 U/ml carboxypeptidase-B eliminated the time-dependence of K_m^F and increased the lysis rate suggesting a role of C-terminal lysines in the progressive clustering of plasmin. This fractal kinetic concept gained structural support from imaging techniques. Atomic force microscopy revealed significant changes in plasmin distribution on patterned fibrinogen surface in line with the time-dependent clustering of fluorescent plasminogen in confocal laser microscopy. These data from complementary approaches supported a mechanism for loss of plasmin activity resulting from C-terminal lysine-dependent redistribution of enzyme molecules on fibrin surface. Our study substantiated in mechanistic terms a fractal kinetic model that describes satisfactorily the action of plasmin on fibrin surface. In this work earlier theoretical predictions for the behavior of surface-acting enzymes and qualitative evidence for spatially constrained migration of plasmin in the network of fibrin fibers converged in a unified concept for quantitative characterization of interfacial fibrinolysis. This concept furthers our understanding of how various factors could affect *in vivo* fibrinolytic rates. The fractal kinetic nature of the interfacial fibrinolysis adds a self-limiting factor to the action of plasmin, which is complementary to the plasma inhibitor-dependent decay of its activity *in vivo* and thus contributes to the higher sensitivity of the fibrinolytic system to regulation at the level of plasminogen activation that supplies new plasmin responding to system demands. In addition to the improved quantitative interpretation of physiological fibrinolysis, this model delineated novel strategies in the ongoing research of direct fibrinolytic enzymes. For example, it predicts that the catalytic efficiency of a protease acting on the surface of fibrin would benefit from retarded clustering of the enzyme, which could be achieved with recombinant modifications of the parent plasmin molecule (optimizing the number of its fibrin-binding sites and their fibrin affinity).

Although most of the work performed within the framework of the project is basic science research, several results bear immediate clinical relevance. In our **paper #11** we performed analysis of the relationships between clinical data and structural characteristics of thrombi. Thrombus samples removed by percutaneous coronary intervention (thrombus aspiration) following acute myocardial infarction (n=101) or surgical open repair of large peripheral arteries (n=50) were processed for scanning electron microscopy or for indirect immunostaining for fibrin and platelet receptor GpIIb/IIIa. We focused on the influence of smoking and accompanying pathological states on the composition of coronary and peripheral arterial thrombi. A significant difference was found in fibrin content of coronary thrombi between smokers and non-smokers. In line with this data, fluorescent fibrin/platelet coverage ratio was significantly lower in non-smokers. No direct influence of smoking was observed on clot RBC occupancy. A non-linear positive dependence of thrombus platelet content on systemic platelet count was observed in both coronary and peripheral thrombi. While the correlation was altered by gender and anti-platelet pre-treatment in peripheral thrombosis patients, the association found in coronary thrombi was stronger in active and former smokers and in patients with

dyslipidaemia. Higher intrathrombotic platelet content tends to be accompanied by thinner fibrin fibers in peripheral thrombi, which correlation is remarkably stronger when dyslipidaemia is present. By multivariable regression analysis, a strong correlation of haematocrit, patient age and clot RBC content was found among hypertensive patients. Leukocyte and RBC count jointly influenced clot platelet content, especially in female, atherosclerotic and non-diabetic peripheral patients. Our new analysis revealed that cigarette smoking and accompanying pathological conditions have pronounced effects on thrombus composition. These observations may help to understand how these conditions relate to arterial thrombosis.

The techniques developed for the evaluation of fibrin ultrastructure proved to be a valuable tool for the examination of the lens capsule structure in the course of ophthalmologic surgery (**papers #12-14**). Although apparently not related to the topic of the project, these results were possible only due to the experience acquired in the sample processing of fibrin clots and thrombi for scanning electron microscopy within the framework of this project.

A set of unpublished results is summarized in the Appendix to this final report. These will be submitted for publication after the completion of the project.

The support from OTKA definitely contributed to the sustainability of the human resources at the hosting research group and the development of their professional career. The full-time employment of Imre Varjú allowed him to gain a PhD degree based on the research performed with OTKA support. The efficient exploitation of the salary support is certified by the international recognition of Dr. Varjú's achievements. He was an invited speaker at the XXVth Congress of the International Society on Thrombosis and Haemostasis, Toronto June 20-June 25, 2015 and he was awarded an EMBO short-term postdoctoral fellowship starting in July 2015, which will be followed by a postdoctoral fellowship granted by the Hungarian Academy of Sciences (start day October 2015). His preliminary results were acknowledged with a prize for the best oral presentation at the 9th symposium of the Young Scientists Association, Vienna 2013 and the best poster presentation at the 22nd Congress on Fibrinolysis and Proteolysis, Marseille 2014. The international recognition of the research supported by OTKA is highlighted also by the two invited talks, which were delivered by the principal investigator (K. Kolev) of the project at the XXIVth Congress of the International Society on Thrombosis and Haemostasis, Amsterdam June 29-July 4, 2013 and the XXVth Congress of the International Society on Thrombosis and Haemostasis, Toronto June 20-June 25, 2015 and the invited review in the state-of-the-art issue of *Journal of Thrombosis and Haemostasis* 2015 (**paper #15**).

Full-length papers with acknowledged support from OTKA

1. Varjú I; Sótonyi P; Machovich R; Szabó L; Tenekedjiev T; Silva M; Longstaff C; Kolev K. Hindered dissolution of fibrin formed under mechanical stress. *J Thromb Haemost* 2011; 9: 979-986
IF5.738

2. Varjú I; Longstaff C; Szabó L; Farkas AZ; Varga-Szabó VJ; Tanka-Salamon A; Machovich R; Kolev K. DNA, histones and neutrophil extracellular traps exert anti-fibrinolytic effects in a plasma environment. *Thromb Haemost* 2015;113(6): 1289-1298
IF5.760

3. Kovács A; Szabó L; Longstaff C; Tenekedjiev K; Machovich R; Kolev K. Ambivalent roles of carboxypeptidase B in the lytic susceptibility of fibrin. *Thromb Res* 2014;133: 80-87
IF2.427

4. Longstaff C, Thelwell C, Williams S, Silva MMCG, Szabó L, Kolev K. The interplay between tissue plasminogen activator domains and fibrin structures in the regulation of fibrinolysis: kinetic and microscopic studies. *Blood* 2011; 117: 661-668

IF: 9.898

5. Wohner N; Sótonyi P; Machovich R; Szabó L; Tenekedjiev K; Silva MMCG; Longstaff C; Kolev K. Lytic resistance of fibrin containing red blood cells. *Arterioscl Thromb Vasc Biol* 2011; 31: 2306-2313

IF6.368

6. Longstaff C; Varjú I; Sótonyi P; Szabó L; Krumrey M; Hoell A; Bóta A; Varga Z; Komorowicz E; Kolev K. Mechanical stability and fibrinolytic resistance of clots containing fibrin, DNA and histones. *J Biol Chem* 2013; 288: 6946-6956

IF4.600

7. Wohner N; Kovács A; Machovich R; Kolev K. Modulation of the von Willebrand factor-dependent platelet adhesion through alternative proteolytic pathways. *Thromb Res* 2012;129: e41-e46

IF3.133

8. Rottenberger Z; Kolev K. Matrix metalloproteinases at key junctions in the pathomechanism of stroke. *Cent Eur J Biol* 2011; 6: 471-485

IF: 1.000

9. Rottenberger Z; Komorowicz E; Szabó L; Bóta A; Varga Z; Machovich R; Longstaff C; Kolev K. Lytic and mechanical stability of clots composed of fibrin and blood vessel wall components. *J Thromb Haemost* 2013; 11: 529-538

IF5.550

10. Varjú I; Tenekedjiev K; Keresztes Z; Pap AE; Szabó L; Thelwell C; Longstaff C; Machovich R; Kolev K. Fractal Kinetic Behavior of Plasmin on the Surface of Fibrin Meshwork. *Biochemistry* 2014; 53: 6348-56

IF3.194

11. Kovács A; Sótonyi P; Nagy AI; Tenekedjiev K; Wohner N; Komorowicz E; Kovács E; Nikolova N; Szabó L; Kovalszky I; Machovich R; Szelid Z; Becker D; Merkely B; Kolev K. Ultrastructure and composition of thrombi in coronary and peripheral artery disease: correlations with clinical and laboratory findings. *Thromb Res* 2015; 135: 760-766

IF2.427

12. Sándor GL; Kiss Z; Bocskai Z; Kolev K; Takács AI; Juhász E; Kránitz K; Tóth G; Gyenes A; Bojtár I; Juhász T; Nagy ZZ. Comparison of the mechanical properties of anterior lens capsule following manual capsulorhexis and femtosecond laser capsulotomy. *J Refract Surg* 2014; **30**(10): 660-664

IF2.781

13. Sándor GL; Kiss Z; Bocskai Z; Kolev K; Takács AI; Juhász E; Kránitz K; Tóth G; Gyenes A; Bojtár I; Juhász T; Nagy ZZ. Comparison of the mechanical properties of anterior lens capsule following femtosecond laser capsulotomy at different energy settings. *J Refract Surg* 2015; **31**(3):153-157

IF2.781

14. Ecsedy M; Sandor GL; Takacs AI; Kranitz K; Kiss Z; Kolev K; Nagy ZZ. Femtosecond laser-assisted cataract surgery in Alport syndrome with anterior lenticonus. *Eur J Ophtalm* 2015; doi: 10.5301/ejo.5000603

IF1.058

15. Longstaff C; Kolev K. Basic mechanisms and regulation of fibrinolysis. *J Thromb Haemost* 2015; 13: S98-S105

IF5.550

Book chapters

Tenekedjiev K, Nikolova N, Kolev K. Applications of Monte Carlo Simulation in Modelling of Biochemical Processes. In: Charles J Mode (Ed.) Applications of Monte Carlo Methods in Biology, Medicine and Other Fields of Science. (ISBN:978-953-307-427-6) Rijeka: InTech Education and Publishing, 2011, pp. 57-76.

Nikolova ND; Toneva-Zheynova D; Kolev K; Tenekedjiev K. Monte Carlo Statistical Tests for Identity of Theoretical and Empirical Distributions of Experimental Data, In: Wai Kin (Victor) Chan (Ed.) Theory and Applications of Monte Carlo Simulations, ISBN: 978-953-51-1012-5, Rijeka: InTech Education and Publishing, 2013, pp. 1-26

Varjú I; Kolev K. Fibrinolysis at the interface of thrombosis and inflammation – the role of neutrophil extracellular traps. In: Kolev K (Ed.) Fibrinolysis and thrombolysis. ISBN 978-953-51-1265-5, Rijeka: InTech Education and Publishing, 2014, pp. 31-59

Appendix
(unpublished results)

Structure and function of trypsin-loaded large unilamellar liposomes

In animal studies, liposome-encapsulated fibrinolytic agents have been shown to offer a number of potentially important advantages compared to conventional drugs. Most trials are done with encapsulated plasminogen activators, which are delivered to and released exactly at the site of the clot. However, due to leakage in the systemic circulatory system, bleeding side effects still remain a disadvantage of liposomal thrombolysis to be overcome. If we consider its fibrinolytic potential of trypsin shown in our earlier work and the massive presence of α_1-antitrypsin in blood that could prevent systemic proteolysis, trypsin could be a suitable candidate for a lytic active ingredient of a liposomal drug delivery system. In our work we examined the structure of the trypsin-loaded liposomes and the liposome-mediated fibrinolysis carried out with trypsin-loaded large unilamellar liposomes (LUVs) in a dynamic, fibrin permeation system.

Methods

Preparation of trypsin loaded LUVs

LUVs consisting of hydrogenated soybean phosphatidyl choline, cholesterol, distearoyl phosphatidyl-ethanolamine PEG2000 and cholesterol sulphate at a molar ratio of 15:4:1:1 were prepared as follows. Constituents were mixed and dissolved in a chloroform/methanol mixture (95:5 volume ratio). After evaporation of the solvent, the lipid film was hydrated with HBS (HEPES buffered saline: 10 mM HEPES, 150 mM NaCl, pH 7.4) containing 10 mg/ml trypsin and stirred for 10 min at 1200 rpm. Formation of unilamellar vesicles was carried out by sonication (three cycles of 30 s at 50-watt, 20-kHz in a Branson Sonifier 250, Branson Ultrasonics Corp., Danbury, CT) followed by ten freeze-thaw cycles (-78 - +42 °C). LUVs were then extruded through a 100-nm pore diameter polycarbonate filter in a Liposofast mini-extruder (Avestin Inc., Ottawa, Canada). Non-encapsulated trypsin and lipid debris were removed by centrifugation for 15 min at 133,000*g* with a Beckman Airfuge 340401 ultracentrifuge followed by resuspending the sediment in HBS. The concentration of phospholipids in the LUV suspension was determined with the fluorescent probe DPH[1]. LUVs were then stored at 4°C until use.

Clot dissolution with trypsin loaded liposomes in a fibrin permeation system

The inner surface of plastic pipette tips were incubated with 1 g/l fibrinogen for 16 h and air-dried. Fibrinogen at 7.5 μM was clotted with 16 nM thrombin in the fibrinogen coated pipette tips. After 70 min of incubation at 37°C, clots were washed thoroughly with HBS to remove unclotted fibrinogen molecules. Trypsin loaded liposomes were centrifuged for 15 min at 133 000 g and resuspended in HBS to eliminate trypsin molecules that leaked out from the vesicles. The enzyme activity of encapsulated trypsin was determined with the small synthetic peptide substrate Spectrozyme-PL at 405 nm with a Beckman DU-7500 spectrophotometer. Liposomes (40 μl) with a phospholipid content of 5 mg/ml and encapsulated trypsin with enzyme activity corresponding to a 0.02 mg/ml trypsin solution, or HBS were then layered over the fibrin clot surface. After the whole volume of liposomal solution was absorbed into

[1] Jouanel, P., Motta, C., Delattre, J., and Dastugue, B. (1980) Clin. Chim. Acta 105, 173–181

the fibrin due to gravitation, flow was maintained and pressure was kept constant by layering 100 µl HBS over the clots. Fractions of 50 µl were collected and their protein concentration was determined by the fluorescamine method[2]. Fractions with the highest protein content were analysed with SDS polyacrylamide gel electrophoresis (SDS PAGE) in a 4-15 % gradient gel under non-reducing conditions, followed by visualization of protein bands with silver staining.

Small angle x-ray scattering (SAXS)

Small-angle X-ray scattering measurements were performed using CREDO, an in-house transmission geometry set-up (Wacha et al., 2014). Samples were filled into thin-walled quartz capillaries of 1.2 mm average outer diameter. After proper sealing, these were placed in a temperature controlled aluminum block, which was inserted into the vacuum space of the sample chamber. Measurements were done using monochromatized and collimated Cu Kα radiation (0.1542 nm wavelength), and the scattering pattern was recorded in the range of 0.23-1.03 nm^{-1} in terms of the scattering variable, q ($(4\pi/\lambda)\sin\Theta$), where 2θ is the scattering angle and λ is the X-ray wavelength). The total measurement times were 7.5 hours for each sample. In order to be able to assess sample and instrument stability during the experiment, the exposures were made in 5 minute units, with frequent sample change and reference measurements. These individual exposures were corrected for beam flux, geometric effects, sample self absorption and instrumental background, as well as calibrated into physical units of momentum transfer (q, nm^{-1}) and differential scattering cross-section (absolute intensity, $cm^{-1}\times sr^{-1}$). The average of the corrected and calibrated scattering patterns was azimuthally averaged to yield a single one-dimensional scattering curve for each sample.

Feigin, L.A., and Svergun, D.I. (1987). Structure Analysis by Small-Angle X-Ray and Neutron Scattering (New York: Plenum Press).
Glatter, O., and Kratky, O. (1982). Small angle x-ray scattering (New York: Academic Press).
Guinier, A., and Fournet, G. (1955). Small-angle scattering of X-rays (New York: John Wiley & Sons, Inc.).
Wacha, A., Varga, Z., and Bóta, A. (2014). CREDO: a new general-purpose laboratory instrument for small-angle X-ray scattering. J. Appl. Crystallogr. *47*, 1749–1754.

Transmission electron microscopy combined by freeze fracture (FF-TEM)

A 1-2 µl droplet of the samples was used for freeze fracturing. The samples were pipetted to the golden sample holder and rapidly freezed in liquid freon then put into liquid nitrogen. Fracturing was performed at 173 K in a Balzers freeze-fracture device (Balzers BAF 400D, Balzers AG, Liechtenstein). The fractured surfaces were etched for 30 s at 173 K. The replicas were made by consecutive platinum and carbon shadowing then washed with surfactant solution and distilled water. Those were transferred to 200 mesh copper grids for transmission electron microscopic (MORGAGNI 268D, FEI, The Netherlands) examination.

Fourier transform infrared spectroscopy (FTIR)

For FTIR spectroscopic study the attenuated total reflection (ATR) technique was used, having a penetration depth of infrared light in the samples in the order of one micrometer, so the investigation in bulk aqueous phase is possible, too.
ATR-FTIR spectroscopic measurements were carried out by means of a Varian 2000 (Scimitar Series) FTIR spectrometer fitted with a diamond attenuated total reflection cell (Specac 'Golden Gate' single reflection ATR unit with active area of 600 x 600 um^2). 5 ul of sample

[2] Anal Biochem 1993; 214:346-348

was spread onto the diamond ATR surface. Room temperature spectra were recorded both as suspension (a cap was used to avoid sample drying) and as dry film (after slowly evaporation of the buffer solvent under ambient conditions). 128 scans were collected at a resolution of 2 cm^{-1}. ATR correction was executed after each data collection. All spectral manipulations were performed using GRAMS/32 software package (Galactic Industries Incorporation, USA).

Results

FF-TEM

The TEM combined by freeze-fracture method provides an excellent possibility to visualize the fractured surfaces of the vesicle systems. The typical fractured surfaces of the nearly spherical shaped vesicles are shown in the Fig TEM-1 obtained in the trypsin containing vesicle system. In this Figure we can observe three types of fractures. Firstly the convex fractured surfaces of the vesicles which are emerged out from the aqueous medium. Secondly we can observe concave areas which are the prints of vesicles broken out entirely from the medium. These two types of fractured creations dispose sharp contours. Moreover, a third type of characteristic fractured surface appears; some vesicles are broken through and their bottom parts remain in the medium. In these cases the contours are not sharp but rather wide and the thickness of the vesicle-wall can be estimated. The vesicle system without trypsin exhibits similar surface morphology and the round-shaped vesicles are the typical formations as it can be observed in Fig. TEM-2/A. Taking a closer look at the electronmicrographs, the outer surface of the vesicles and their prints proved to be smooth because the limited roughness of the electronmicrographs is the consequence of the platinum grains with a mean size of approx. 1-2 nm-s which is below the size of trypsin (Figs. TEM-2/A, B). In the trypsin containing vesicles similar surface character can be observed in the outer convex and concave surfaces (Fig. TEM-3/A), but in the third type of fracturing a feature also appears. Closely packed small grains with a diameter of about 3 nm-s, presumably the trypsin molecules, coat the inner surface of bilayer shells as it can be revealed in higher magnification in Fig TEM-3/B. This observation indicates that the trypsin molecules are attached to the inner surface of vesicles characteristically and these enzyme molecules are not loosely and interiorly closed in the vesicles.

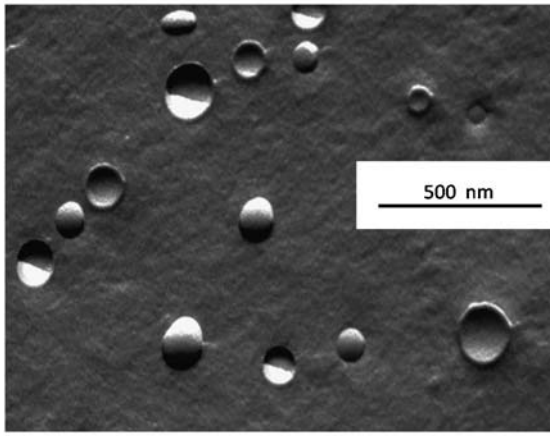

Fig. TEM-1 Typical surface morphology of the nearly spherical shaped vesicles in the trypsin containing system. Three types of fractures can be observed; i) convex fractured surfaces of

the vesicles emerged out from the aqueous medium ii) concave areas of prints of vesicles broken out iii) bottom parts of remaining vesicles broken through entirely

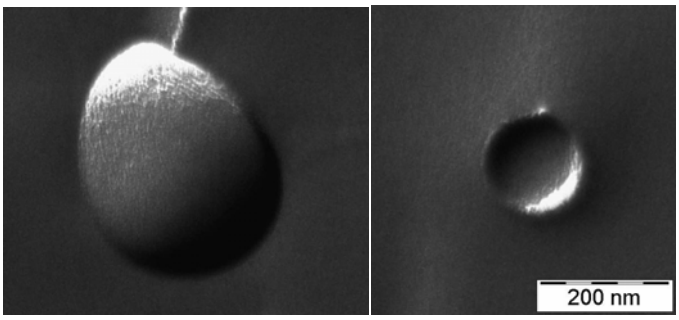

Fig. TEM-2/A,B The surface morphology of vesicle without trypsin. The outer surface (A) and the inner surface of vesicles (B, a vesicle broken through entirely) are typically smooth.

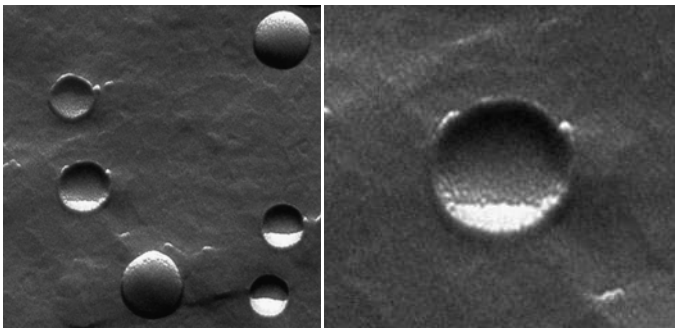

Fig. TEM-3/A,B The surface morphology of vesicles containing trypsin. The all three types of fractured surfaces can be observed (A), inner surface of vesicle containing closely packed trypsin (B).

SAXS

To follow the changes in the layer structure of the sterically stabilized vesicles induced by the added trypsin, small angle X-ray scattering (SAXS) measurements were applied. We have investigated the empty vesicles, the trypsin containing vesicles and the trypsin in adequate concentration (the same as it was in vesicles system). The one-dimensional scattering patterns of the samples can be observed in Fig. SAXS-1. Only the shape of the SAXS curve of trypsin solution differs from that of the vesicle systems. It is degreasing monotonously in function of scattering variable and has a declination in the q-range between 0.2 – 2 nm^{-1}, corresponding to the nearly spherical shape and to its ca. 3 nm diameter. In the beginning range of the scattering curve the significant intensity indicates aggregates in the aqueous milieu. In the other samples also intense scattering appear in the beginning range of scattering variable which is degreasing

monotonously. This character is typical for complex systems containing heterodisperse domains in the size range from several nanometers up to hundreds of nanometers. The vesicle systems exhibit nearly similar scattering, both have the characteristic broad "hump" in the q-range from 0.4 to 2 nm^{-1}, which is the consequence of the quadrate of lipid bilayer form factor. However, there is a slight but important difference of the scattering patterns. The local minimum of the curve of trypsin containing vesicle is not so deep than in the case of that of empty vesicles. In the first approach we can interpret the SAXS curve of the trypsin containing vesicle as the sum of scatterings of its constituents. The results of this assumption can also be seen in Fig. SAXS-1. The sum of scattering of constituents and the scattering of the measured complex vesicle differs from each other. Especially, the difference is significant in the regime of the form factor indicating the change in bilayer structure and in the same time the organization between the structural units, namely between the lipid bilayer and the trypsine.

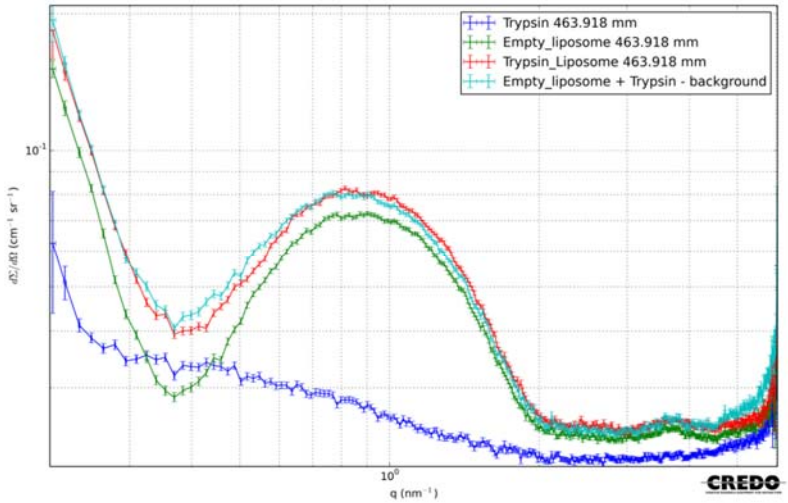

Fig. SAXS-1 The one-dimensional scattering patterns of sterically stabilized vesicles with (red) and without (green) trypsin in buffer. The scattering curve of the adequate solution of trypsin is also plotted.

This feature of scattering curves can be reconstructed by a centrosymmetrical shell model whereby an approximate description of the layer structure becomes possible. Neglecting the interactions between vesicles and supposing their spherical forms the scattering intensity can be calculated by the '2 Gaussian' symmetric model. In this model one Gaussian function represents the polar head group region of the lipid bilayers, while another one the electron density of guest molecules (in our cases the PEG chains of pegylated lipid and trypsin) located in the vicinity of the head groups. It must be mentioned that the model contains a third Gaussian for the hydrocarbon chain region of lipid double layers consequently, but not mentioned in the model name. Using this model we have already characterized of the layer structure of sterically stabilized vesicles and pointed out that the PEG chains form cohesive layers at both (in outer and inner sides of vesicles) and their thickness can be approximated around 4 nm.

In the present study the best fit yields an inner and an outer shell region whereby we intend to characterize the location of trypsin constituents. The results indicate very different thickness for the outer and inner shell regions. The thickness of the outer shell of trypsin containing system is similar to that of system without trypsin, therefore we may conclude that the outer region does not have trypsin and it represents the PEG chains of the pegylated lipid, while trypsin molecules must be concentrated in the inner leaflets, whereby its thickness

became significantly wider. The shell model and the important structural parameters are summarized in Fig. SAXS/2.

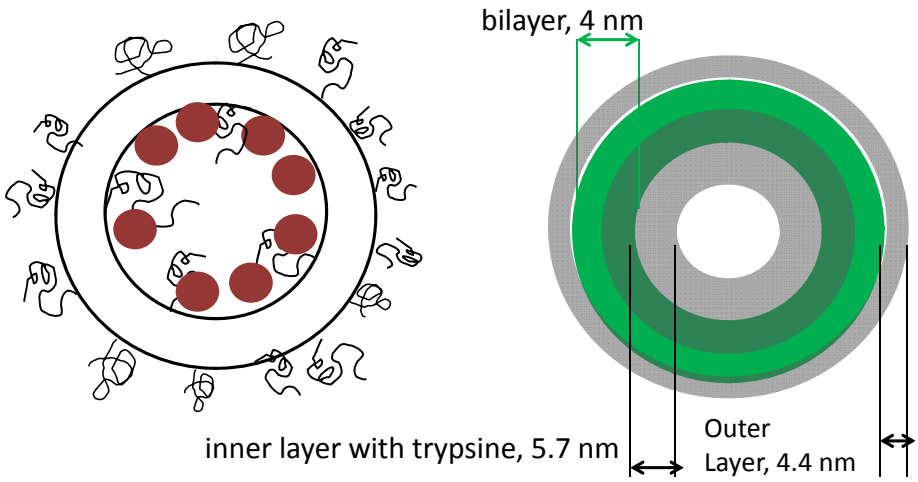

Fig. SAXS-2 Shell model for interpretation of the SAXS data. The scattering curve can be described with a thick inner shell containing closely packed trypsin molecules.

FT-Infrared Spectroscopy

Dry film spectra:

Figure IR1 shows the ATR-FTIR spectra of 'empty' and trypsin loaded SSL.

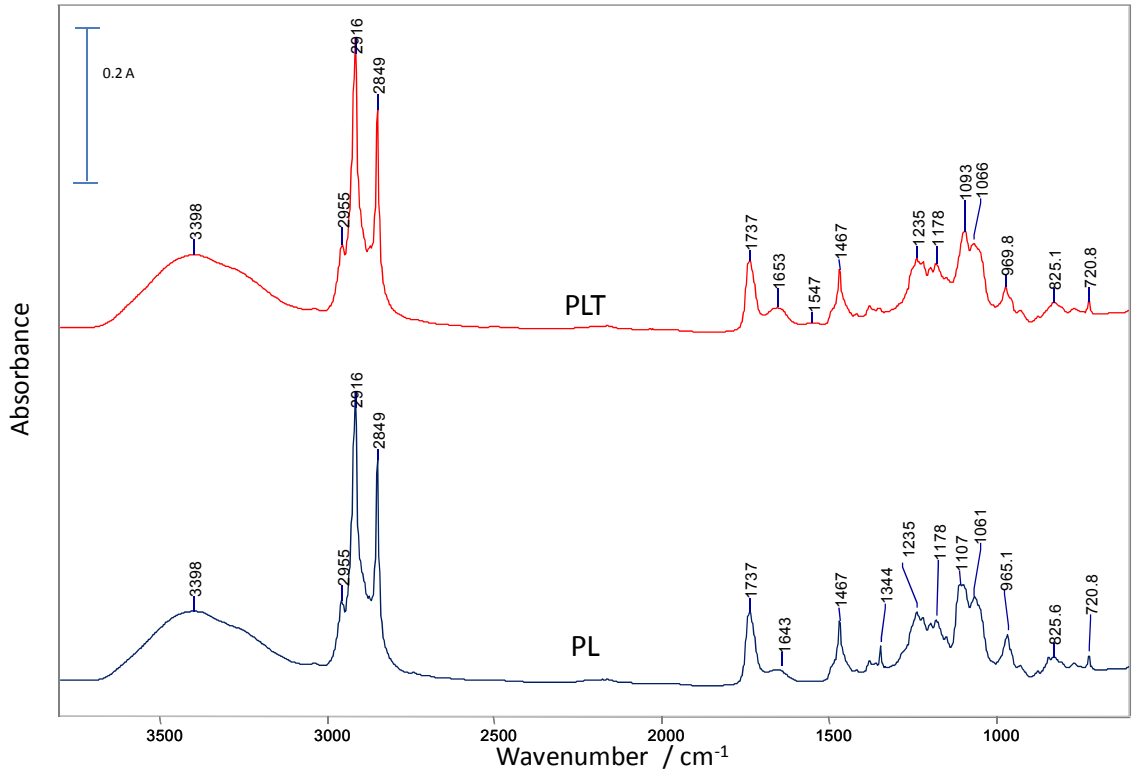

Fig. IR1 Dry film spectra of trypsin loaded (PLT) and empty (PL) SSLs.

At first look no significant differences can be observed. Subtracted spectra, however, reveals the presence of Amide I and Amide II bands at 1653 and 1547 cm^{-1}, respectively, corresponding to the presence of trypsin (Figure IR2). Negative bands of PLT-PL (loaded SSL subtracted by empty SSL) resembles to the spectrum of polyethylene glycol (PEG), due to the feasible differences in PEG content of empty SSL (PL) and trypsin loaded SSL (PLT).

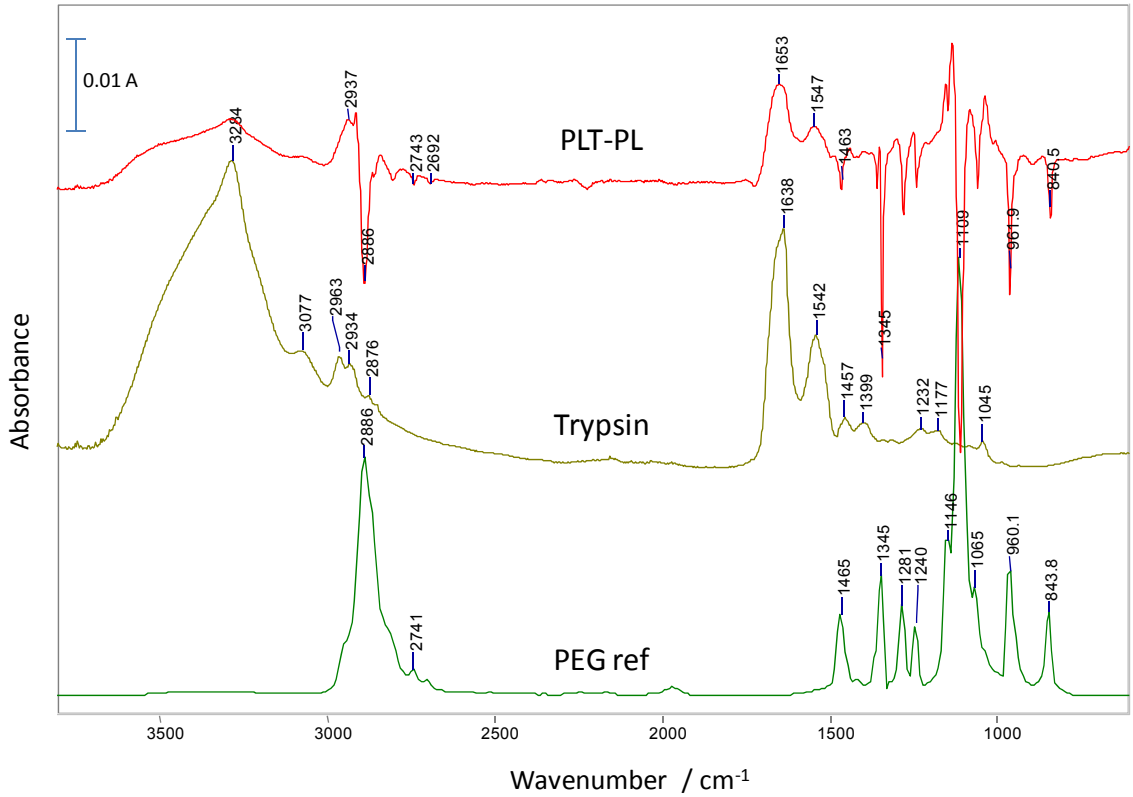

Fig. IR2 Subtracted trypsin loaded SSL spectrum (PLT-PL), compared to the spectrum of trypsin solution (Trypsin) and PEG reference (PEGref).

FTIR spectroscopy is widely applied to study protein secondary structure and aggregation. In particular, the Amide I band (1700-1600 cm^{-1}), corresponding mainly to the C=O stretching vibration of the peptide bond (~80%), is sensitive to the protein backbone conformational changes. Figure IR3 shows the Amide I spectral region of trypsin spectra before (in solution) and after encapsulation, together with the second derivative spectra. Trypsin is a so called β-protein with dominant content of β-sheets and β-turns conformation [J Kong, S Yu, Acta Biochim Biophys Sinica 2007 (839) 549-559]. After encapsulation, the relative amount of β-sheet conformers is slightly decreased, while the band component corresponding to α-helix structure is slightly increased, reflected also by shape of the Amide I band envelope.

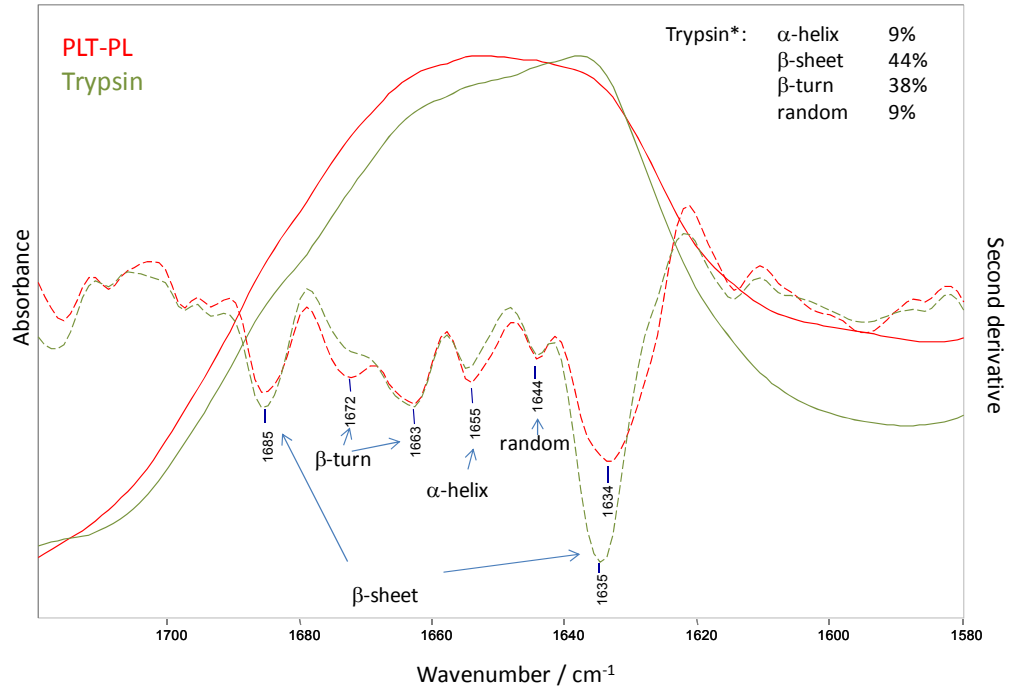

Fig. IR3 Amide I spectral region of trypsin before (green lines) and after encapsulation (red lines); full lines – dry film spectra, stacked lines – second derivatives. The second derivatives of the measured spectra were obtained by the Savitsky-Golay method (third grade polynomial, 5 smoothing points).

Suspension spectra:

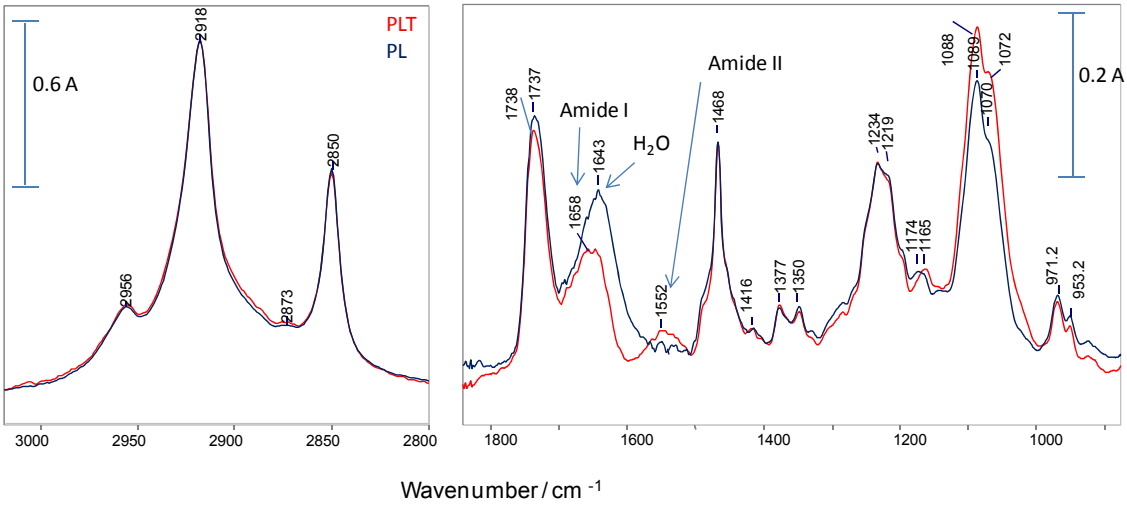

Fig. IR4 Suspension spectra of trypsin loaded (PLT) and empty (PL) SSls (spectra are background corrected by buffer spectrum).

The C-H stretching region of the IR spectra (3020-2800 cm^{-1}) involves mostly the fatty acyl chains of the lipids (Figure IR4). No differences were witnessed for trypsin loaded and empty

SSLs suggesting that the order/disorder of the acyl chains remains intact. As to the lipid headgroup spectral region (1800-900 cm^{-1}), again no changes in the phosphate vibrations ($\nu_{as}PO_2^-$ at 1234 cm^{-1}, $\nu_sPO_2^-$ at 1088 cm^{-1} and νR-O-P-O-R' around 1070 cm^{-1}) and in the antisymmetric C-N^+ stretching vibrations (971 cm^{-1}) of the choline groups can be revealed.
The lipidic carbonyl ester group is situated in the interfacial region of the lipid bilayer and is a potential H-bonding formation site. In highly hydrated phospholipid bilayers this band splits in two overlapping component: a high wavenumber band around 1742 cm^{-1} of the non-hydrogen bonded C=O groups and a low wavenumber band around 1728 cm^{-1} due to the hydrogen bonding of the C=O groups [RNAH Lewis, RN McElhaney, BBA 1828 (2013) 2347–2358]. Detailed analysis of the νC=O band around 1737 cm^{-1} (Figure IR5) indicates an increase of relative amount of free C=O subpopulation: A (νC=O H-bonded) / A (νC=O free) decrease from 2.5 for PL to 1.8 for PLT. It seems plausible that the trypsin is located close to the lipid hydrophilic/hydrophobic interface and expulses water molecules from lipid ester carbonyl region. This fact is further supported by the decreased water deformation band intensity (at 1643 cm^{-1}) in the PLT suspension spectrum (see Figure IR4).

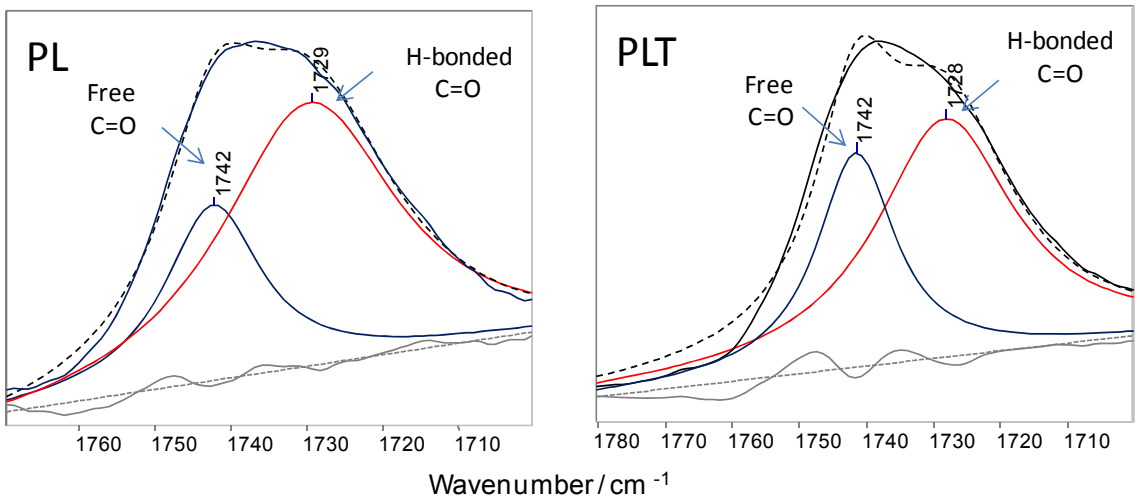

Fig. IR5 Lipid ester carbonyl stretching band region for empty (PL) and trypsin loaded (PLT) liposomes: the solid black lines are the measured spectra; the blue and the red lines are the fitted bands corresponding to intact and H-bonded C=O groups, respectively. Band positions for curve fitting were determined using the second derivative, band shapes were approximated by Lorentzian functions. The intensities and the bandwidth of each component were allowed to vary until the minimal χ^2 parameter was reached. After the fitting procedure, the relative contribution of a particular component was calculated from the integrated areas of the individual components.

As a summary, we can state that the presence trypsin molecules do not disturb the acyl chain ordering of the SSLs lipid bilayer. Instead, the encapsulated trypsin might be situated close to the lipid hydrophilic/hydrophobic interface and expulses water molecules from lipid ester carbonyl moiety.

Fibrinolytic efficiency of trypsin-loaded liposomes

Trypsin loaded liposomes were layered over pure fibrin clots clotted in pipette tips, through which fluid flow was ensured by adding HBS on the top and collecting fractions at the lower orifice of the tips. Protein content of fractions were determined and plotted against the eluted volume.

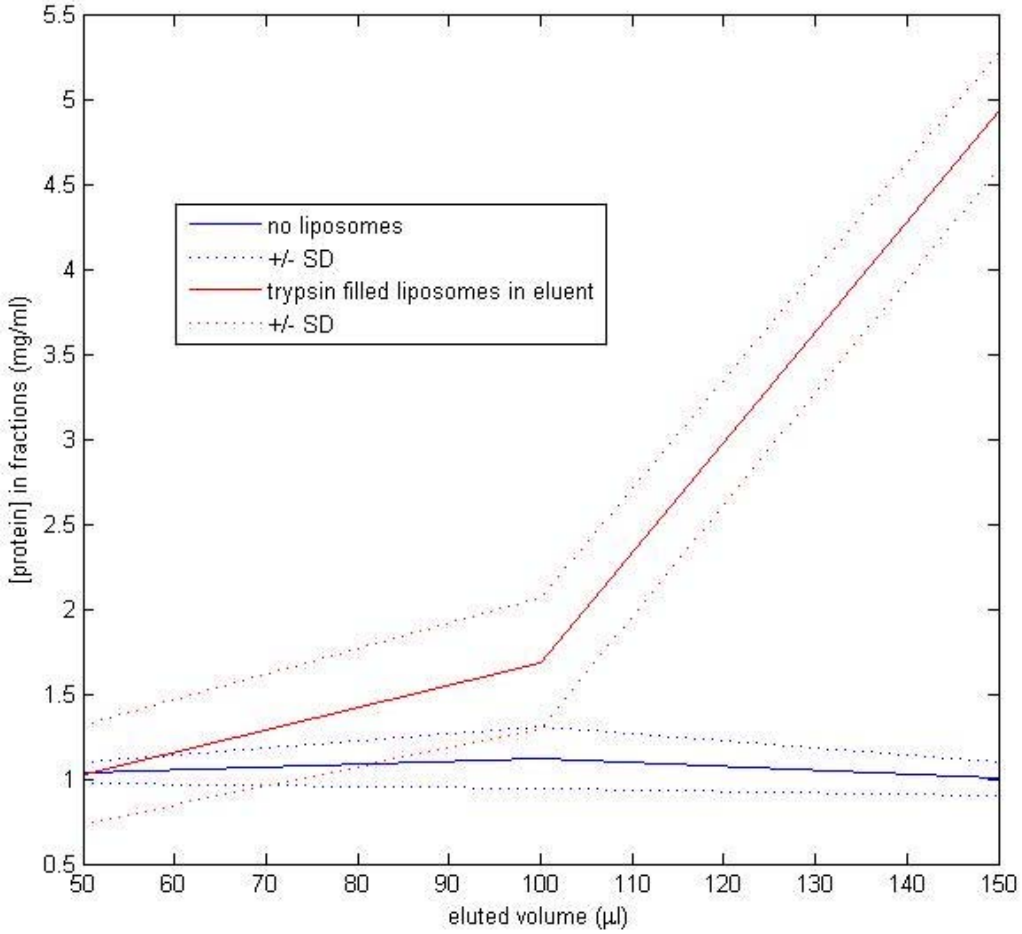

The increasing protein concentrations in the successional fractions points to the fact that liposomal trypsin was released and exerted its fibrinolytic activity on the clot.

SDS PAGE was performed to examine the protein size distribution of the 3rd fraction in three parallel samples (A, B, C).

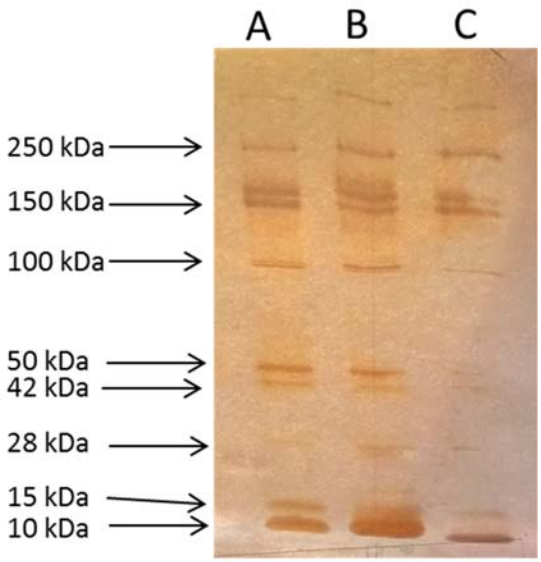

A plasmin-like degradation pattern of fibrin was observed with different types of fibrin degradation products, which evidences that the protein content of fractions with the highest protein concentrations originated exclusively from fibrin degraded by trypsin.